Enhanced Superconductivity in FeSe Thin Films on LiF Substrates

Zhiyu Huang(黄智宇)[1,2†], Xuewei Wang(王雪玮)[1,2†], Qiuyan Shi(史秋艳)[1,2], Zhanyi Zhao(赵展艺)[1,2], Changhong Yuan(袁长红)[1,2], Yutong Wang(王宇彤)[1,2], Yating Jiang(姜亚婷)[1,2], Yuhan Jin(金昱晗)[1,2], Beiyi Zhu(朱北沂)[1], Jie Yuan(袁洁)[1,2,3], Fedor Kusmartsev[4], Atsutaka Maeda[5,6], Zefeng Lin(林泽丰)[1*], Qihong Chen(陈其宏)[1,2*], and Kui Jin(金魁)[1,2,3]

[1]*Beijing National Laboratory for Condensed Matter Physics, Institute of Physics, Chinese Academy of Sciences, Beijing 100190, China*
[2]*School of Physical Sciences, University of Chinese Academy of Sciences, Beijing 100049, Chin*
[3]*Songshan Lake Materials Laboratory, Dongguan 523808, China*
[4]*College of Engineering and Physical Sciences, Khalifa University, PO Box 51133 Abu Dhabi, United Arab Emirates*
[5]*Department of Basic Science, The University of Tokyo, 3-8-1 Komaba, Meguro-ku, Tokyo 153-8902, Japan*
[6]*The Physical Society of Japan, 2-31-22-5F Yushima, Bunkyo-ku, Tokyo 113-0034, Japan*

(Received 17 November 2025; accepted manuscript online 27 February 2026)

FeSe films have attracted extensive research interest in iron-based superconductors owing to their highly tunable superconducting properties. Here, we fabricated a series of FeSe films with various thicknesses on LiF substrates using pulsed-laser deposition. The onset superconducting transition temperature T_c^{onset} reaches ∼22 K for ∼20–50 nm-thick films, which is nearly three times that of bulk FeSe and much higher than values previously reported for FeSe films on fluoride substrates. Additionally, T_c^{onset} increases anomalously as the film thickness decreases. Transport measurements reveal no clear signatures of interfacial electron doping from the LiF substrate. Structural characterizations indicate an out-of-plane *c*-axis expansion accompanied by an in-plane lattice contraction in FeSe/LiF films. The large thermal expansion coefficient of LiF implies that the enhanced T_c originates from strong in-plane compressive strain induced during post-growth cooling. This study provides an interpretation of the varying superconducting properties in FeSe films and offers valuable insights into further enhancing T_c through heterostructure engineering.

DOI: 10.1088/0256-307X/43/4/040706 CSTR: 32039.14.0256-307X.43.4.040706

1. Introduction. The iron-based superconductor FeSe has attracted considerable attention owing to its highly tunable superconducting transition temperature (T_c). Although bulk FeSe exhibits a relatively low T_c of ∼9 K at ambient pressure,[1] its superconductivity can be significantly enhanced to ∼40 K through external pressure,[2–4] chemical intercalation,[5–7] or electrostatic gating.[8–10] In thin-film form, FeSe also displays remarkable superconducting properties. For example, FeSe films can reach a maximum T_c of ∼15 K.[11,12] In particular, monolayer FeSe films grown by molecular beam epitaxy on $SrTiO_3$ (STO) substrates exhibit superconducting gap-opening temperatures exceeding 65 K,[13] while transport measurements have revealed T_c values above 40 K.[14,15] More recently, ultrathin FeSe films grown on STO by pulsed-laser deposition (PLD) have achieved T_c values above 30 K.[16,17] These findings make FeSe films a key platform for studying interface-enhanced superconductivity.

The enhancement of T_c in FeSe/STO systems is widely attributed to interfacial effects, such as electron transfer[18–20] from the STO substrate to FeSe and electron–phonon coupling mediated by STO phonons.[21,22] Consequently, superconductivity in these systems is generally believed to be confined near the interface rather than exhibiting bulk-like behavior.[13,16,23] In contrast, FeSe films with conventional thicknesses, particularly those grown on CaF_2 and LiF substrates, exhibit higher T_c values than bulk FeSe and display robust, nonvolatile bulk superconductivity. Compared with bulk FeSe, these films often show an enlarged *c*-axis lattice parameter,[12,24] indicating the presence of strain within the films. The origin of this strain remains an open question crucial to understanding the mechanism of superconductivity enhancement in FeSe films and for advancing their practical applications.

In this paper, we fabricated high-quality FeSe films with thicknesses ranging from 20 to 200 nm on LiF substrates. The films exhibit an enhanced T_c with decreasing thickness, achieving a maximum T_c^{onset} of ∼22 K for the 20–50 nm-thick films, which cannot be explained by interfacial electron doping from LiF. By correlating the thickness dependence of the lattice parameters and transport properties, our results suggest that the enhanced T_c originates from a strong in-plane compressive strain imposed by the LiF substrate during post-growth cooling, enabled by the exceptionally large thermal expansion coefficient of LiF.

†These authors contributed equally to this work.
*Corresponding authors. Email: linzefeng@iphy.ac.cn; qihongchen@iphy.ac.cn

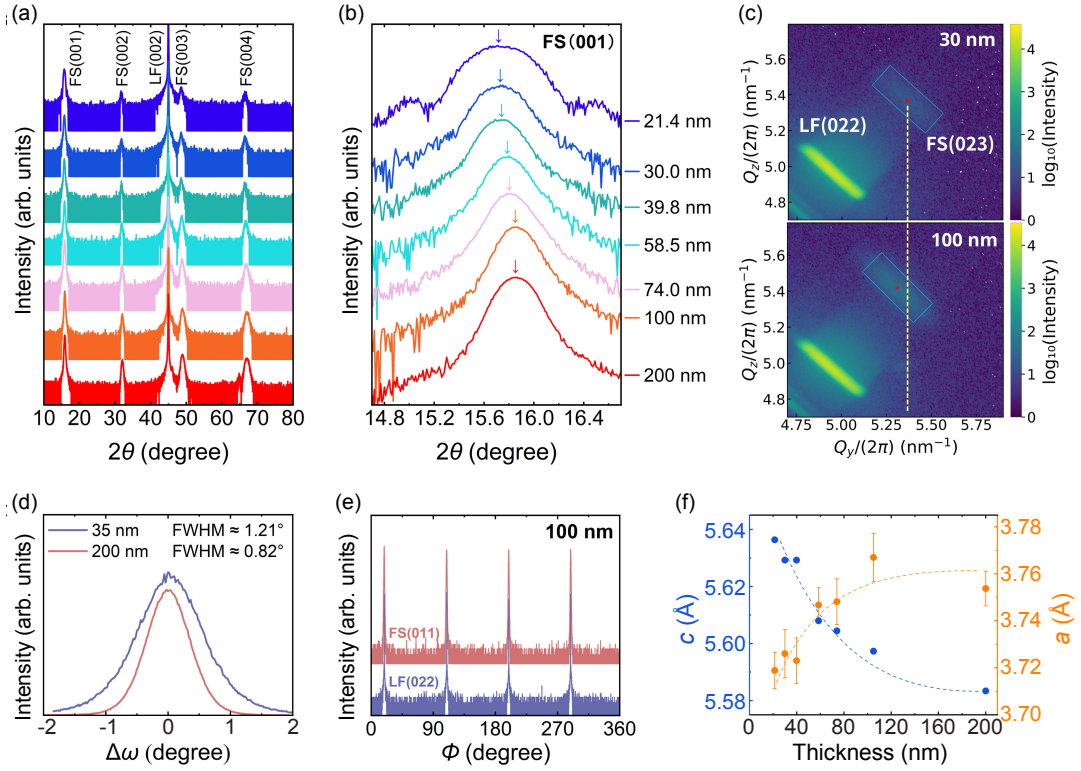

Fig. 1. Structural characterization of FeSe/LiF films. (a) XRD θ–2θ scans of FeSe/LiF films with different thicknesses. (b) Enlarged view of the FeSe (001) diffraction peak from (a). (c) RSM measurements showing the FeSe (023) and LiF (022) peaks for the 30-nm-thick and 100-nm-thick films. (d) Rocking curves of the FeSe (001) peak for the 30-nm-thick and 100-nm-thick films. (e) ϕ-scan of the FeSe (011) reflection. (f) Thickness dependence of the out-of-plane lattice parameter c (from θ–2θ scans) and the in-plane lattice parameter a (from RSM measurements). The dashed lines are guides to the eye and do not represent a quantitative fit.

2. Methods. FeSe films were grown on LiF substrates using PLD. A polycrystalline FeSe target with nominal composition Fe:Se = 1:0.93 was prepared by solid-state reaction and sintering. An Nd:YAG laser ($\lambda = 355$ nm) was used to ablate the target for film growth, with a pulse energy of 200 mJ and a repetition rate of 4 Hz. During deposition, the substrate temperature was set to 325 ℃ at a target–substrate distance of 60 mm. Growth was carried out in high vacuum (better than 2×10^{-4} Pa) to prevent oxidation. After deposition, samples were cooled to room temperature. By controlling the deposition time, we prepared a series of FeSe films with thicknesses ranging from 20 to 200 nm.

The film thicknesses, out-of-plane and in-plane crystalline structure, and phase purity were characterized by x-ray reflectivity (XRR), θ–2θ x-ray diffraction (XRD), and reciprocal space mapping (RSM) using a Rigaku SmartLab x-ray diffractometer with Cu $K\alpha$ radiation. Film thickness was determined by XRR, which is suitable for films thinner than 100 nm. For films thicker than 100 nm, the thickness was estimated from the number of laser pulses used during growth. Electrical transport properties, including the longitudinal resistance and the Hall effect, were measured using a standard Hall-bar geometry in a Physical Property Measurement System (PPMS, Quantum Design). Diamagnetic measurements were performed using a two-coil mutual-inductance device.

3. Results and Analysis. Figure 1(a) shows out-of-plane θ–2θ XRD scans of FeSe films with varying thicknesses grown on (00l)-oriented LiF substrates. All FeSe/LiF films exhibit uniform (00l)-oriented diffraction peaks with no observable impurity phases, indicative of good out-of-plane alignment. In Fig. 1(b), the FeSe (001) diffraction peak shifts to lower angles as the thickness decreases. Pronounced Laue fringes appear for the ∼21.4 nm film, indicating a flat surface and uniform thickness. Figure 1(d) shows the rocking curves of the (001) reflection for two films with different thicknesses. Both curves exhibit slightly larger full widths at half maximum (FWHM) than those reported for FeSe films on CaF_2 substrates,[12] signifying stronger lattice distortion and a higher dislocation density in FeSe/LiF, which may result from the large mismatch between FeSe and LiF. The FWHM decreases with increasing thickness, reflecting partial strain relaxation and improved out-of-plane crystalline alignment. Despite the large mismatch, high-quality epitaxial alignment is confirmed by a fourfold rotational symmetry in the ϕ-scan measurement of the FeSe (011) reflection, as shown in Fig. 1(e).

To further track the thickness evolution of the lattice, we carried out RSM measurements on FeSe/LiF films. Representative maps around the FeSe (023) and LiF (022) reflections are shown in Fig. 1(c). The thickness-dependent in-plane a-axis parameters extracted from the

RSM dataset are summarized in Fig. 1(f). Across the entire thickness range, the in-plane lattice constant remains smaller than the bulk FeSe value ($a = 3.772$ Å), indicating an overall in-plane compressive strain in FeSe/LiF, which becomes more pronounced as the film thickness decreases. Consistently, the FeSe (001) peak in Fig. 1(b) shifts to lower angles (and broadens) upon reducing thickness, implying an expansion of the out-of-plane lattice. As summarized in Fig. 1(f), the c-axis lattice parameter increases markedly with decreasing thickness, accompanied by an overall reduction of the in-plane a-axis, consistent with a Poisson-type elastic response linking in-plane compression to out-of-plane expansion. We note that the in-plane a values derived from RSM generally carry larger uncertainties than the out-of-plane c values extracted from θ–2θ scans, because the asymmetric geometry is more sensitive to instrumental alignment and peak fitting, and typically yields weaker film signals. Nevertheless, the RSM results robustly capture the same thickness trend expected from the strain picture. Therefore, in the following discussion, we primarily use the more accurately determined c-axis parameter as the structural metric to correlate with the superconducting properties.

Figures 2(a) and 2(b) illustrate the temperature dependence of the normalized resistance $R(T)$ for FeSe/LiF films with thicknesses ranging from 21.4 to 200 nm. All films exhibit metallic behavior at high temperatures and superconductivity at low temperatures. Films thicker than 90 nm show a sharp superconducting transition, with $T_c^{\rm onset}$ above 16 K and $T_c^{\rm zero} \sim 12$ K, consistent with previous reports on high-quality films grown on LiF or CaF_2 substrates.[12] Here, $T_c^{\rm onset}$ is determined as the crossing point of the extrapolated normal-state resistance and a linear fit to the steepest part of the transition, and $T_c^{\rm zero}$ as the temperature at which the resistance reaches zero. As the thickness decreases into the 50–90 nm range, $T_c^{\rm onset}$ increases to ∼18 K, while $T_c^{\rm zero}$ remains near 12 K. Meanwhile, the $R(T)$ curves display two distinct superconducting transitions, implying the presence of two superconducting components. This observation is further supported by the broadened diffraction peaks within this thickness range, as shown in Fig. 1(b). Intriguingly, when the thickness is further reduced to below 50 nm, the superconducting transition sharpens again, and $T_c^{\rm onset}$ and $T_c^{\rm zero}$ increase to ∼22 K and ∼19 K, respectively, significantly higher than the previously reported values.[12] The slight reduction in T_c observed for the 21 nm-thick film may originate from the degradation caused by air exposure. Nevertheless, as shown in Fig. 2(c), the overall trend indicates that T_c increases with decreasing film thickness.

A similar trend of T_c enhancement with decreasing thickness has been reported for FeSe films grown on atomically flat STO substrates.[25–27] The microscopic mechanism underlying the enhanced T_c in these systems is extensively thought to be associated with charge transfer[18,20,28] and electron–phonon coupling[21,22] at the FeSe/STO interface: an oxygen-vacancy-rich STO substrate can supply additional electrons to the FeSe layer and also provide interfacial optical phonons that couple to FeSe electrons. However, such a thickness dependence of T_c is unusual for FeSe films grown on fluoride substrates or other substrates.[29–31] In previous work, a reduction in T_c has usually been observed in FeSe films or thin flakes as the thickness decreases, commonly attributed to reduced dimensionality and to increased disorder induced by interfacial strain and defects.[32] As shown in Fig. 2(a), a slight resistivity upturn in the $R(T)$ curves, appearing prior to the superconducting transition, becomes more pronounced as the film thickness decreases, suggesting increased disorder and possible weak-localization effects in thinner FeSe/LiF films. This interpretation is further supported by the reduced residual-resistivity ratio (RRR) in the thinner samples, extracted from the $R(T)$ curves, as shown in Fig. 2(e). Increased disorder is generally expected to weaken superconductivity, which contrasts with our findings.

During film growth, Li atoms may diffuse from the LiF substrate into the FeSe layer, providing electron doping that contributes to the enhanced T_c. One potential mechanism is that Li intercalates into the FeSe layer and forms new phases with higher T_c, such as Li_xFeSe,[33] which has previously been realized in the gated FeSe flakes using a solid-ion conductor. However, the XRD patterns of our FeSe/LiF films show no evidence of new phases. An alternative mechanism is a Li-induced interfacial reduction. An analogous phenomenon has been observed in surface alkali-metal dosing of FeSe.[34–36] Previous studies have demonstrated that the ionic-liquid gating can significantly enhance the T_c of FeSe films while simultaneously improving RRR through electron doping.[10] By contrast, in our FeSe/LiF films, the RRR does not increase with decreasing thickness, despite the expected stronger interfacial doping effect in thinner films. To further examine the possibility of substrate-induced electron doping, we measured the temperature dependence of the Hall coefficient R_H for FeSe/LiF films with different thicknesses, as shown in Fig. 2(f). At low temperatures, all FeSe/LiF films exhibit a positive R_H, consistent with hole-dominated transport in a compensated semimetal. Notably, the thinner films with higher T_c show a larger positive R_H than the thicker films at the same temperature. This behavior is qualitatively opposite to that observed in electron-doped FeSe systems.[8] As shown by the data for an ion-gated FeSe/LiF film (200 nm) included for comparison,[37] increasing electron doping drives R_H downward and eventually toward negative values. In contrast, in our thinner FeSe/LiF films, R_H increases with decreasing thickness and increasing T_c, indicating that the superconducting enhancement is not accompanied by electron doping. Together with the reduced RRR in thinner films, these Hall results strongly suggest that interfacial electron transfer from LiF is unlikely to be the primary origin of the observed T_c enhancement.

An alternative explanation for the enhanced T_c is the strain effect between the FeSe layer and the substrate. Figure 2(d) compares the c-axis lattice parameters of the

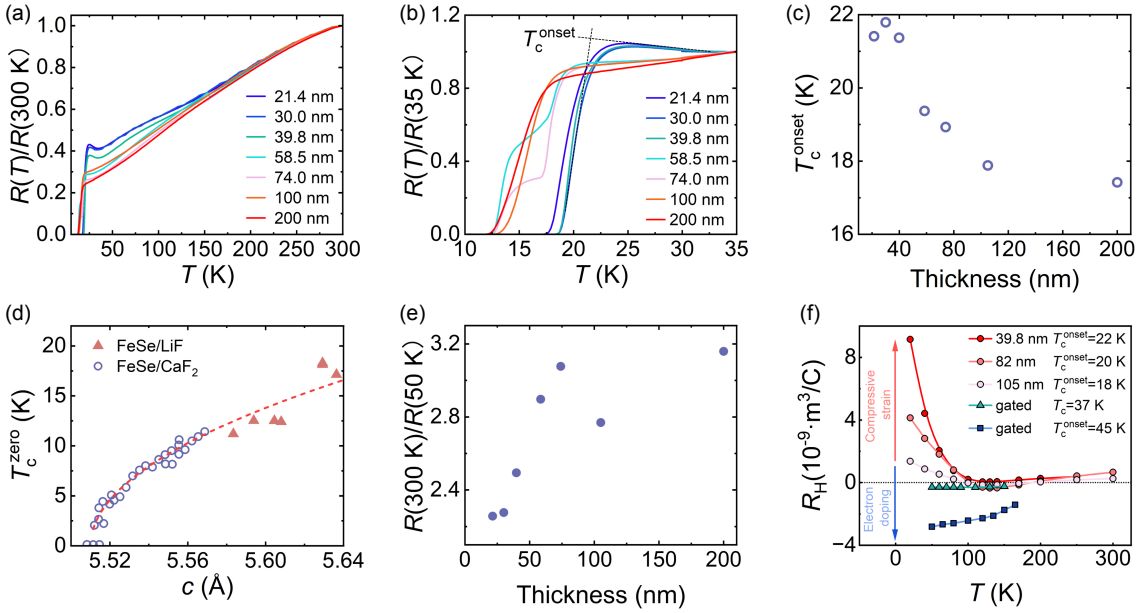

Fig. 2. Electrical transport properties of FeSe/LiF films with various thicknesses. (a) Temperature dependence (5–300 K) of the normalized resistance $R(T)/R(300\,\mathrm{K})$ for FeSe/LiF thin films of various thicknesses. All films undergo the superconducting transitions at low temperatures. (b) Enlarged view of the normalized resistance across the superconducting transition region (10–35 K). (c) T_c^{onset} versus thickness. (d) T_c^{zero} for FeSe/LiF films versus c-axis lattice parameter c compared with $FeSe/CaF_2$ data.[38] (e) RRR $R(300\,\mathrm{K})/R(50\,\mathrm{K})$ versus thickness, indicating reduced metallicity in thinner films. (f) Temperature dependence of the Hall coefficient R_{H} for FeSe/LiF films with different thicknesses (39.8, 82, and 105 nm). For comparison, data for electron-doped FeSe/LiF films and FeSe thin flakes obtained by ionic-liquid gating are included (triangle and square symbols adapted from Refs. [37] and [8], respectively). The dashed line marks $R_{\mathrm{H}} = 0$.

FeSe/LiF films in this study with those of $FeSe/CaF_2$ films reported in the literature.[38] A guide-to-the-eye fit follows the empirical relation,[38]

$$T_c \propto \sqrt{c - c_0}, \quad c_0 = 5.51\,\text{Å},$$

originally extracted for $FeSe/CaF_2$ films. The T_c values of the FeSe/LiF samples exhibit a nearly monotonic correlation with the c-axis lattice parameter, supporting the view that lattice distortion is the primary driver of the T_c enhancement. This behavior is consistent with prior reports on FeSe films grown on other substrates[24] and on $FeSe_{1-x}Te_x$ films,[39,40] in which T_c often correlates with out-of-plane lattice expansion under epitaxial strain. It is also broadly compatible with high-pressure studies on bulk FeSe,[2–4] in which T_c is strongly enhanced under compression. The simultaneous expansion of the c-axis and contraction of the a- and b-axes naturally alters the electronic band structure,[41,42] which in turn suppresses nematicity and modifies the superconducting properties.[38]

4. Discussion. Notably, the FeSe/LiF films exhibit an unprecedentedly large c-axis compared with the previously reported FeSe films, indicating substantial in-plane lattice contraction in the FeSe layer relative to bulk FeSe. This is counterintuitive because LiF has a larger in-plane lattice parameter than FeSe and would therefore be expected to impose tensile strain on the FeSe layer. A similar behavior is observed for $FeSe/CaF_2$ films. In principle, such tensile strain could elongate the a- and b-axes and compress the c-axis of FeSe, which could in turn lower T_c. Yet, the opposite trend is observed in this study.

Interestingly, among the FeSe films grown on various substrates, those deposited on LiF and CaF_2 exhibit a much larger c-axis lattice constant and a higher T_c, despite the non-negligible lattice mismatch between FeSe and these fluoride substrates. In particular, LiF imposes a relatively large mismatch (+6.45%). By contrast, FeSe films grown on $LaAlO_3$ substrates anomalously exhibit a markedly smaller c-axis and a much lower T_c, even though $LaAlO_3$ imposes a compressive strain and a negligible lattice mismatch. There are several mechanisms to account for the c-axis expansion in $FeSe/CaF_2$. Previous TEM/STEM-EDX studies have proposed that elemental interdiffusion at the interface of CaF_2 and FeSe can result in out-diffusion of Se into CaF_2 during the initial growth[43] or formation of an ∼3 nm-thick interfacial CaSe layer.[31] Both processes deplete Se in the adjacent FeSe layer and can strongly affect the stoichiometry and superconducting properties. However, these explanations cannot fully account for the enhanced T_c observed in FeSe/LiF, suggesting the involvement of additional mechanisms.

When evaluating strain effects in thin films, it is essential to consider the lattice evolution of both the films and substrates during the heating and cooling stages of growth. It has been demonstrated that when a film and its substrate exhibit mismatched thermal expansion, post-deposition cooling causes them to contract at different rates, thereby inducing additional in-plane compressive or tensile strains in the film. In particular, because CaF_2 has a relatively large thermal expansion coefficient $\alpha_{300\,\mathrm{K}}$,

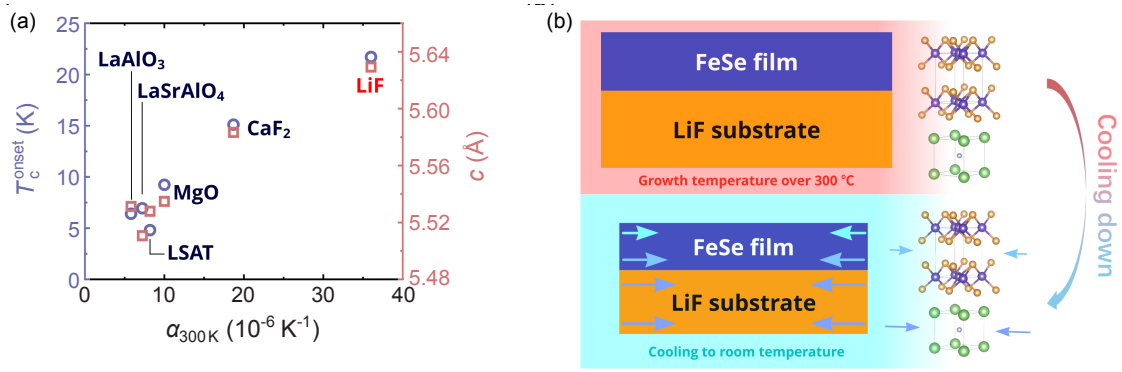

Fig. 3. Thermal expansion mismatch drives strain-enhanced superconductivity in FeSe films. (a) T_c^{onset} and c vs the 300 K thermal expansion coefficient ($\alpha_{300\,K}$) across different substrates.[12] Substrates with larger $\alpha_{300\,K}$ tend to yield higher T_c^{onset}, consistent with a strain-driven enhancement mechanism. (b) Schematic illustration of thermally induced strain in FeSe/LiF heterostructures. During deposition at high temperatures (above 300 ℃), the FeSe film and LiF substrate approach a quasi-equilibrium state. Upon cooling, the large thermal contraction of LiF imposes strong in-plane compressive strain on the FeSe layer, resulting in in-plane lattice contraction and c-axis expansion.

this differential contraction tends to impose an in-plane compressive strain on the film, leading to a reduced a- and b-axis lattice constants.[44–48] To further understand the influence of substrate thermal expansion on FeSe films, figure 3(a) summarizes the $\alpha_{300\,K}$ of several representative substrates, together with the corresponding c-axis lattice parameters and the reported optimal T_c values for FeSe grown on several representative substrates.[12] Interestingly, LiF and CaF_2 possess larger $\alpha_{300\,K}$ values than other substrates, with LiF showing the largest among them. Moreover, the c-axis and T_c values show a positive correlation with $\alpha_{300\,K}$ among various substrates, implying that the thermal expansion-induced strain plays an important role in modulating the FeSe lattice and T_c. Therefore, a possible physical picture to account for the c-axis expansion and enhanced T_c in FeSe/LiF is illustrated schematically in Fig. 3(b). Before FeSe deposition, the LiF substrate is heated to the growth temperature (∼325 ℃) and its lattice expands significantly owing to the large $\alpha_{300\,K}$. During FeSe deposition, the large lattice mismatch between FeSe and LiF leads to the formation of defects and dislocations, which accommodate the mismatch and help maintain partial in-plane and out-of-plane alignment without substantial c-axis variation. Upon completion of the growth, as the sample cools down to room temperature, the LiF substrate undergoes pronounced lattice contraction, exerting a strong compressive stress on the FeSe layer and thereby causing a substantial expansion of its c-axis. The presence of defects and dislocations stabilizes this lattice configuration, rendering the structural modification nonvolatile. Consequently, the stronger compressive strain leads to an increase in T_c in FeSe/LiF.

When the FeSe layer is thin (e.g., <50 nm), the compressive strain can affect nearly the entire lattice, leading to a higher T_c^{onset} of ∼22 K. Below 50 nm, the film can become more uniformly clamped by the substrate, so the strain state may approach a quasi-saturated regime where further thickness reduction produces smaller incremental changes in lattice parameters. As the FeSe thickness increases, the c-axis lattice parameter gradually decreases [see Fig. 1(f)], suggesting a progressive relaxation of the strain from the LiF substrate. When the thickness reaches an intermediate value (∼50–90 nm), the upper portion (likely above ∼40 nm) of the FeSe film experiences a weaker strain and thus exhibits a lower T_c^{onset} (∼18 K), while the bottom layer remains in a high-T_c state. This explains why films within this thickness range display two distinct superconducting transitions. With further increases in thickness beyond 90 nm, the T_c^{onset} values decrease to ∼16 K, possibly because the upper layers impose tensile strain on the bottom layer. This indicates that the superconductivity enhancement is governed by a strain-dominated layer with a finite thickness, rather than an effect confined to only a few atomic layers at the interface. We emphasize that thermal expansion mismatch is likely not the only control parameter. The final strain state is governed by the combined effect of lattice mismatch, thermal expansion mismatch, defect density, strain-relaxation pathways, interfacial chemistry, and the (possibly thickness-dependent) formation and kinetics of misfit dislocations.[49] Such competition can lead to a steady strain state rather than a continuous relaxation toward the bulk limit. Nevertheless, the combined structural-transport correlations and the cross-substrate trend make thermal mismatch-induced compressive strain the most consistent interpretation of our observations. Further investigations are required to verify this scenario, for instance by performing temperature-dependent (ideally *in situ*) measurements to monitor the lattice evolution of the FeSe film during growth and subsequent cooling. More broadly, lattice distortion and the resulting strain state may also affect the magnetism and spin excitations of FeSe.[50–52] It will therefore be important in future work to correlate such lattice evolution with magnetism and spin excitations. Nevertheless, our findings provide a feasible route to improve the superconducting properties of materials by utilizing the difference in thermal expansion coefficients between the film and the substrate to generate sufficiently strong strain, thereby significantly modulating the lattice and enhancing T_c.

Remarkably, this enhancement is nonvolatile, offering valuable insights for the optimization of superconducting heterostructures and coated conductors.

5. Conclusion. In summary, we fabricated a series of high-quality FeSe films with varying thicknesses on LiF substrates using PLD. The FeSe/LiF films exhibit a pronounced T_c enhancement with decreasing thickness, reaching a record T_c^{onset} ∼22 K, the highest value reported for FeSe grown on fluoride substrates. Structural characterization reveals a strong in-plane lattice contraction accompanied by out-of-plane (c-axis) expansion. Transport measurements show no clear signature of interfacial electron doping. By comparing the lattice parameters of FeSe films with the thermal expansion coefficients of their substrates, we proposed that compressive strain arising from thermal expansion mismatch would significantly expand the c-axis of the FeSe layer and enhance the T_c. Our work provides a plausible interpretation for the higher T_c in FeSe grown on fluoride substrates, and offers valuable insight into improving superconductivity through the design of heterostructures with mismatched thermal expansion properties.

Acknowledgements. We thank Lihong Yang for RSM measurements and Yaxun He for helpful discussion. This work was supported by the National Key R&D Program of China (Grant Nos. 2022YFA1403900, 2022YFA1403000, and 2022YFA1603900), the National Natural Science Foundation of China (Grant Nos. 12374141, 12225412, 52588301, and 12504169), the Chinese Academy of Sciences (CAS) President's International Fellowship Initiative (Grant Nos. 2024DM0018 and 2025PG0007), CAS Project for Young Scientists in Basic Research (Grant No. 2022YSBR-048), and the Open Research Fund of the Pulsed High Magnetic Field Facility, Huazhong University of Science and Technology (Grant No. WHMFC2024001). This work was also technically supported by Synergetic Extreme Condition User Facility (SECUF, https://cstr.cn/31123.02.SECUF).

References

[1] Hsu F C, Luo J Y, Yeh K W, Chen T K, Huang T W, Wu P M, Lee Y C, Huang Y L, Chu Y Y, Yan D C, and Wu M K 2008 *Proc. Natl. Acad. Sci. USA* **105** 14262
[2] Medvedev S, McQueen T M, Troyan I A, Palasyuk T, Eremets M I, Cava R J, Naghavi S, and Safa-Sefat A S 2009 *Nat. Mater.* **8** 630
[3] Sun J P, Matsuura K, Ye G, Shimozawa M, Mizukami Y, Matsubayashi K, Yamashita S, Uwatoko Y, Shibauchi T, and Matsuda Y 2016 *Nat. Commun.* **7** 12146
[4] Sun J P, Ye G Z, Shahi P, Yan J Q, Matsuura K, Kontani H, Zhang G M, Zhou Q, Sales B C, Shibauchi T, Uwatoko Y, Singh D J, and Cheng J G 2017 *Phys. Rev. Lett.* **118** 147004
[5] Guo J G, Jin S F, Wang G, Wang S C, Zhu K X, Zhou T T, He M, and Chen X L 2010 *Phys. Rev. B* **82** 180520
[6] Burrard-Lucas M, Free D G, Sedlmaier S J, Wright J D, Cassidy S J, Hara Y, Corkett A J, Lancaster T, Baker P J, Blundell S J, and Clarke S J 2013 *Nat. Mater.* **12** 15
[7] Huang Y L, Feng Z P, Ni S L, Li J, Hu W, Liu S B, Mao Y Y, Zhou H X, Zhou F, Jin K, Wang H B, Yuan J, Dong X L, and Zhao Z X 2017 *Chin. Phys. Lett.* **34** 077404
[8] Lei B, Cui J H, Xiang Z J, Shang C, Wang N Z, Ye G J, Luo X G, Wu T, Sun Z, and Chen X H 2016 *Phys. Rev. Lett.* **116** 077002
[9] Wang W K, Liu Y, Yang J Y, Du H F, Ning W, Ling L S, Tong W, Qu Z, Yang Z R, Tian M L, and Zhang Y H 2016 *Chin. Phys. Lett.* **33** 057401
[10] Jiang X Y, Qin M Y, Wei X J, Xu L, Ke J Z, Zhu H P, Zhang R Z, Zhao Z Y, Liang Q M, Wei Z X, Lin Z, Feng Z P, Chen F C, Xiong P Y, Yuan J, Zhu B Y, Li Y M, Xi C Y, Wang Z S, Yang M, Wang J F, Xiang T, Hu J P, Jiang K, Chen Q H, Jin K, and Zhao Z X 2023 *Nat. Phys.* **19** 365
[11] Imai Y, Sawada Y, Asami D, Nabeshima F, and Maeda A 2016 *Physica C* **530** 24
[12] Feng Z P, Yuan J, He G, Hu W, Lin Z F, Li D, Jiang X Y, Huang Y L, Ni S L, Li J, Zhu B Y, Dong X L, Zhou F, Wang H B, Zhao Z X, and Jin K 2018 *Sci. Rep.* **8** 4039
[13] Wang Q Y, Li Z, Zhang W H, Zhang Z C, Zhang J S, Li W, Ding H, Ou Y B, Deng P, Chang K, Wen J, Song C L, He K, Jia J F, Ji S H, Wang Y Y, Wang L L, Chen X, Ma X C, and Xue Q K 2012 *Chin. Phys. Lett.* **29** 037402
[14] Zhang W H, Sun Y, Zhang J S, Li F S, Guo M H, Zhao Y F, Zhang H M, Peng J P, Xing Y, Wang H C, Fujita T, Hirata A, Li Z, Ding H, Tang C J, Wang M, Wang Q Y, He K, Ji S H, Chen X, Wang J F, Xia Z C, Li L, Wang Y Y, Wang J, Wang L L, Chen M W, Xue Q K, and Ma X C 2014 *Chin. Phys. Lett.* **31** 017401
[15] Zhao D P, Cui W Q, Liu Y W, Gong G M, Zhang L G, Jia G H, Zang Y Y, Hu X P, Zhang D, Wang Y L, Li W, Ji S H, Wang L L, He K, Ma X C, and Xue Q K 2024 *Nat. Commun.* **15** 3369
[16] Kobayashi T, Nakagawa H, Ogawa H, Nabeshima F, and Maeda A 2023 *J. Phys. Condens. Matter* **35** 41LT01
[17] Zhao Z Y, Wei Z X, Yu X D, Dong W F, Huang J R, Chen C R, Feng Z P, Qin M Y, Wang X W, Cao S G, Huan Q, Li Y M, Yuan J, Zhu B Y, Chen Q H, Sun Y J, Wang L L, Qian T, and Jin K 2024 *Phys. Rev. B* **110** L140507
[18] He S L, He J F, Zhang W H, Zhao L, Liu D F, Liu X, Mou D X, Ou Y B, Wang Q Y, Li Z, Wang L L, Peng Y Y, Liu Y, Chen C Y, Yu L, Liu G D, Dong X L, Zhang J, Chen C T, Xu Z Y, Chen X, Ma X C, Xue Q K, and Zhou X J 2013 *Nat. Mater.* **12** 605
[19] Cheng F J, Zhang Y M, Fan J Q, Song C L, Ma X C, and Xue Q K 2023 *Chin. Phys. Lett.* **40** 086801
[20] Kobayashi T, Ogawa R, and Maeda A 2025 *Phys. Rev. B* **112** 094525
[21] Lee J J, Schmitt F T, Moore R G, Johnston S, Cui Y T, Li W, Yi M, Liu Z K, Hashimoto M, Zhang Y, Lu D H, Devereaux T P, Lee D H, and Shen Z X 2014 *Nature* **515** 245
[22] Zhang C F, Liu Z K, Chen Z Y, Xie Y W, He R H, Tang S J, He J F, Li W, Jia T, Rebec S N, Ma E Y, Yan H, Hashimoto M, Lu D H, Mo S K, Hikita Y, Moore R G, Hwang H Y, Lee D H, and Shen Z X 2017 *Nat. Commun.* **8** 14468
[23] Lin Z F, Tu S J, Xu J, Shi Y J, Zhu B Y, Dong C, Yuan J, Dong X L, Chen Q H, Li Y M, Jin K, and Zhao Z X 2022 *Sci. Bull.* **67** 1443
[24] Nabeshima F, Kawai M, Ishikawa T, Shikama N, and Maeda A 2018 *Jpn. J. Appl. Phys.* **57** 120314
[25] Tan S Y, Zhang Y, Xia M, Ye Z, Chen F, Xie X, Peng R, Xu D F, Fan Q, Xu H C, Jiang J, Zhang T, Lai X C, Xiang T, Hu J P, Xie B P, and Feng D L 2013 *Nat. Mater.* **12** 634
[26] Ichinose A, Nabeshima F, Tsukada I, Hanawa M, Komiya S, Akiike T, Imai Y, and Maeda A 2013 *Supercond. Sci. Technol.* **26** 075002
[27] Peng R, Xu H C, Tan S Y, Cao H Y, Xia M, Shen X P, Huang Z C, Wen C, Song Q, Zhang T, Xie B P, Gong X G, and Feng D L 2014 *Nat. Commun.* **5** 5044

[28] Zhang H M, Zhang D, Lu X W, Liu C, Zhou G Y, Ma X C, Wang L L, Jiang P, Xue Q K, and Bao X H 2017 *Nat. Commun.* **8** 214

[29] Schneider R, Zaitsev A G, Fuchs D, and von Löhneysen H 2012 *Phys. Rev. Lett.* **108** 257003

[30] Nabeshima F, Imai Y, Hanawa M, Tsukada I, and Maeda A 2013 *Appl. Phys. Lett.* **103** 172602

[31] Qiu W B, Ma Z Q, Patel D, Sang L N, Cai C B, Shahriar Al Hossain M, Cheng Z X, Wang X L, and Dou S X 2017 *ACS Appl. Mater. Interfaces* **9** 37446

[32] Farrar L S, Bristow M, Haghighirad A A, McCollam A, Bending S J, and Coldea A I 2020 *npj Quantum Mater.* **5** 29

[33] Lei B, Wang N Z, Shang C, Meng F B, Ma L K, Luo X G, Wu T, Sun Z, Wang Y, Jiang Z, Mao B H, Liu Z, Yu Y J, Zhang Y B, and Chen X H 2017 *Phys. Rev. B* **95** 020503

[34] Miyata Y, Nakayama K, Sugawara K, Sato T, and Takahashi T 2015 *Nat. Mater.* **14** 775

[35] Wen C H P, Xu H C, Chen C, Huang Z C, Lou X, Pu Y J, Song Q, Xie B P, Abdel-Hafiez M, Chareev D A, Vasiliev A N, Peng R, and Feng D L 2016 *Nat. Commun.* **7** 10840

[36] Seo J J, Kim B Y, Kim B S, Jeong J K, Ok J M, Kim J S, Denlinger J D, Mo S K, Kim C, and Kim Y K 2016 *Nat. Commun.* **7** 11116

[37] Zhang X, Feng Z P, Wei X J, Lin Z F, Jiang X Y, Hu W, Wei Z X, Qin M Y, Xu J, Xiong R, Shi J, Yuan J, Zhu B Y, Chen Q H, and Jin K 2021 *Phys. Rev. B* **103** 214505

[38] Feng Z P, Zhang H, Yuan J, Jiang X Y, Wu X X, Zhao Z Y, Xu Q H, Stanev V, Zhang Q H, Yang H X, Gu L, Meng S, Weng S M, Chen Q H, Takeuchi I, Jin K, and Zhao Z X 2024 *Quantum Front.* **3** 12

[39] Huang S X, Chien C L, Thampy V, and Broholm C 2010 *Phys. Rev. Lett.* **104** 217002

[40] Kong W D, Liu Z G, Wu S F, Wang G, Qian T, Yin J X, Richard P, Yan L, and Ding H 2015 *Chin. Phys. Lett.* **32** 087401

[41] Phan G N, Nakayama K, Sugawara K, Sato T, Urata T, Tanabe Y, Tanigaki K, Nabeshima F, Imai Y, Maeda A, and Takahashi T 2017 *Phys. Rev. B* **95** 224507

[42] Nakajima M, Ohata Y, and Tajima S 2021 *Phys. Rev. Mater.* **5** 044801

[43] Tsukada I, Ichinose A, Nabeshima F, Imai Y, and Maeda A 2016 *AIP Adv.* **6** 095314

[44] Lei Q Y, Golalikhani M, Yang D Y, Withanage W K, Rafti A, Qiu J, Hambe M, Bauer E D, Ronning F, Jia Q X, Weiss J D, Hellstrom E E, Wang X F, Chen X H, Williams F, Yang Q, Temple D, and Xi X X 2014 *Supercond. Sci. Technol.* **27** 115010

[45] He J, Jia J H, Liu Y Y, Chen Q, Xing X P, Jiang K, Ning X K, Hu J P, Liu D F, Ma X C, and Xue Q K 2016 *Sci. Rep.* **6** 28390

[46] Iida K, Grinenko V, Kurth F, Ichinose A, Tsukada I, Ahrens E, Pukenas A, Chekhonin P, Skrotzki W, Teresiak A, Hühne R, Aswartham S, Wurmehl S, Mönch I, Erbe M, Hänisch J, Holzapfel B, Drechsler S L, and Efremov D V 2016 *Sci. Rep.* **6** 28390)

[47] Yuan F F, Iida K, Grinenko V, Chekhonin P, Pukenas A, Skrotzki W, Sakoda M, Naito M, Sala A, Putti M, Yamashita A, Takano Y, Shi Z, Nielsch K, and Hühne R 2017 *AIP Adv.* **7** 065015

[48] Hänisch J, Iida K, Hühne R, and Tarantini C 2019 *Supercond. Sci. Technol.* **32** 093001

[49] Moridi A, Ruan H H, Zhang L, and Liu M 2013 *Int. J. Solids Struct.* **50** 3562

[50] Liu R X, Nakamura M, Kamazawa K, and Lu X Y 2024 *Chin. Phys. Lett.* **41** 067401

[51] Pelliciari J, Karakuzu S, Song Q, Arpaia R, Nag A, Rossi M, Li J M, Yu T L, Chen X Y, Peng R, García-Fernández M, Walters A C, Wang Q, Zhao J, Ghiringhelli G, Feng D L, Maier T A, Zhou K J, Johnston S, and Comin R 2021 *Nat. Commun.* **12** 3122

[52] Cao B J, Huang C, Jiang L Z, Pan Y F, Shi D N, Fan J Y, Ma C L, and Zhu Y 2025 *Chin. Phys. Lett.* **42** 070714